Oil & Natural Gas Technology

DOE Award No.: DE-FE0013889

Quarterly Research Performance Progress Report (Period ending 09/30/2015)

THCM Coupled Model For Hydrate-Bearing Sediments: Data Analysis and Design of New Field Experiments (Marine and Permafrost Settings)

Project Period (10/1/2013 to 09/30/2016)

Submitted by:

Marcelo Sanchez Project PI

Texas A&M University
DUNS #: 847205572
College Station, TX
979-862-6604
msanchez@civil.tamu

Prepared for:
United States Department of Energy
National Energy Technology Laboratory
Submission date: 11/10/2015

Office of Fossil Energy

DISCLAIMER

ACCOMPLISHMENTS

The experimental study of hydrate bearing sediments has been hindered by the very low solubility of methane in water (lab testing), and inherent sampling difficulties associated with depressurization and thermal changes during core extraction. This situation has prompted more decisive developments in numerical modeling in order to advance the current understanding of hydrate bearing sediments, and to investigate/optimize production strategies and implications. The goals of this research is to addresses the complex thermo-hydro-chemo-mechanical THCM coupled phenomena in hydrate-bearing sediments, using a truly coupled numerical model that incorporates sound and proven constitutive relations, satisfies fundamental conservation principles. This tool will allow us to better analyze available data and to further enhance our understanding of hydrate bearing sediments in view of future field experiments and the development of production technology.

ACCOMPLISHED

The main accomplishments for this first period address Tasks 5, 6 and 7 of the original research plan, and include:

- Update of constitutive equations.
- Update of THCM-Hydrate.
- Numerical analyses.
- Incorporation of additional THCM-Hydrate code modifications.
- Production Optimization of Future Field Studies.

Training

The training of the two PhD students working in this project has continued during this period. Mr. Xuerui (Gary) Gai was hired at the start of the project and his activities have been related to the use of code "THCM-Hydrate"; which is the numerical tool under development in this project. In the last few months his research has focused on the mechanical modeling of Hydrate Bearing Sediments (HBS). Mr. Mehdi Teymouri was hired at the beginning of the second year of the project. His training was initially associated with gaining a better understanding on physical properties of HBS; HBS behavior and hydrate dissociation; and numerical and analytical methods in hydrates research. His research has focused on sand production issues associated with gas production from methane hydrate reservoirs. Both students have progressed positively with their coursework at their respective universities.

Literature review

The literature review (Task 2) was completed in a previous period.

Update of Update of THCM-Hydrate

The update of the constitutive laws for hydrate-bearing marine sediments and HBS in the permafrost (i.e. Task 3) was completed in a previous period.

Close-form analytical solutions

The review on the main governing evolution laws, parameters, dimensionless ratios and simplifying assumptions for HBS dissociation (i.e. Task 4) was completed in the previous period.

Numerical analyses
The numerical analyses to solve field production experiments as boundary value problems have continued in this period.

The mechanical constitutive model has been upgraded to include the effect of gas hydrate dissociation during the analyses. Additional and recent experimental tests involving gas hydrates dissociation have been used to validate the model. A numerical algorithm for its implementation has been developed. The main results are presented in page 6.

In parallel progresses have been made in the modeling of methane production experiments from pressurized cores. Large scale models are also being developed to simulate real production tests. Finally, the modeling of sand production during HBS depressurization is another topic in which progress has been made in this period.

Plan - Next reporting period
We will advance analytical and numerical fronts to enhance our code to solve coupled THCM problems involving with HBS, with renewed emphasis on simulating the natural processes under *in-situ* conditions and gas production. Special emphasis will be placed on issues associated with sand production
.

Milestones for each budget period of the project are tabulated next. These milestones are selected to show progression towards project goals.

	Milestone Title Planned Date and Verification Method	Actual Completion Date	Comments
Title Related Task / Subtasks Planned Date Verification method	Complete literature review 2.0 / 2.a March 2014 Report	March 2014	Completed
Title Related Task / Subtasks Planned Date Verification method	Complete updated Constitutive Equations 2.0 / 2.b & 2.c June 2014 Report (with preliminary validation data)	July 2014	Completed
Title Related Task / Subtasks Planned Date Verification method	Validate new THCM constitutive equations 3.0 / 3.a, 3.b & 3.c September 2014 Report (with first comparisons between experimental and numerical results)	September 2014	Completed
Title Related Task / Subtasks Planned Date Verification method	Complete close-form analytical solutions 4.0 / 4.a & 4.b February 2015 Report (with analytical data)	February 2015	Completed
Title Related Task / Subtasks Planned Date Verification method	Complete numerical analyses 5.0 / 5.a, 5.b & 5.c July 2015 Report (with analytical and numerical data)	July 2015	Progressing as planned
Title Related Task / Subtasks Planned Date Verification method	Complete THCM-Hydrate code modifications 6.0 / 6.a Originally: June 2015. Extended to May 2016 Report (with numerical data)	March 2016	Progressing as planned
Title Related Task / Subtasks Planned Date Verification method	Complete production optimization 7.0 / 7.a, 7.b, 7.c, 7.d & 7.e Originally: September 2015. Extended to September 2016. Report (with numerical data)	September 2016	Progressing as planned

1. Mechanism analysis of HISS-MH model

The performance of the proposed mechanical model for gas hydrate sediments (i.e. HISS-MH), was evaluated in the previous project report (i.e. Sanchez et al. 2015) against available experimental data involving a variety of tests, some of them published quite recently The model has been extended now to model the mechanical behavior of HBS during hydrate dissociation. Recently published experimental results have been adopted to validate the propose approach.

In this report, a numerical analysis performed to further investigate the plastic mechanisms incorporated in this model to simulate the behavior gas hydrate sediments at constant hydrate saturation is discussed first. The 'cementing pore-habit' case reported in Masui et al. (2005) is adopted for this analysis. The mechanical modeling of HBS during hydrate dissociation is a crucial component to properly simulate gas production strategies. The second part of this report is advocated to this aspect, focusing on the study of cases involving gas hydrate dissociation.

1.1 Cementing case

Three experiments carried out by Masui et al. (2005) were selected to validate the proposed model. A triaxial compression test using pure Toyoura sand (i.e. with no hydrate) was selected, plus two more experiments involving synthetic specimens, one of them with hydrate in pore-filling dominating pore-habit and the other one in which the effect of the hydrate was mainly cementing. The main parameters adopted for the numerical analysis are presented in Table 1, where M is the slope of critical line in the *q-p'* space; λ and k are the slope of the 'normal compression' and 'unloading/reloading' lines in the *e-log(p')* space, respectively; p_c is the preconsolidation pressure, a and γ are constants; m is the parameter related to the transition from compressive to dilative volume change; S_H is the hydrate saturation, α and β are constants that describe the degree of hydrate contribution to the hardening law; μ is the degradation parameter; and η is a sub-loading parameter that controls the plastic deformations before yielding. The porosity values (n) reported by Masui et al. (2005) were between 37.7 and 42.4% and the hydrate saturation was practical identical in both tests (i.e., S_H=0.409 for the pore-filling case and S_H=0.410 for the cementing one).

Table 1. Soil parameters adopted in the modeling of Toyoura sand specimens

Properties	Pure sand	Pore-filling	Cementing
M	1.47	1.47	1.47
λ	0.36	0.36	0.36
κ	0.024	0.024	0.024
p_c (MPa)	6	6	6
m	3	3	3
a	1	1	1
γ	1/9	1/9	1/9
S_H	0	0.409	0.41
α	-	15	30
β	1.6	1.6	1.6
μ	-	1.5	3.5
η	45	45	45

Figure 1 presents the deviatoric stress (q) versus axial strain relationship and volumetric behavior of the selected tests showing with symbols the experiments and with lines the model outputs. A marked increase in the initial stiffness and strength is observed in the pore-filling and cementing samples. It is clear that the enhancement in stiffness, strength and dilatancy is higher in cementing samples. The degradation parameter μ depends on hydrate morphology. The critical state parameters (such as the slopes of critical state line, the normal compression line, and unloading/reloading line) are the same for both cases since they are considered independent of hydrate morphology

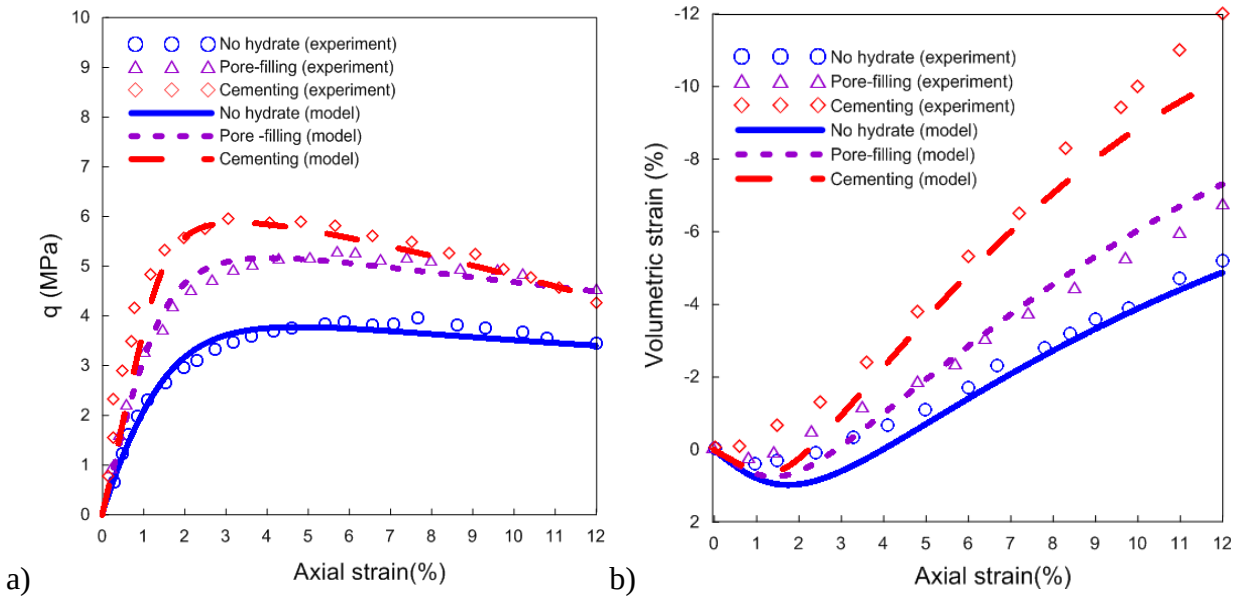

Figure 1 Modeling the drained triaxial tests on pure Toyoura sand and hydrate samples using the HISS MH model: a) stress strain behavior, b) volumetric response. Experimental data after Masui et al. (2005).

It can be observed that the model is able to capture very satisfactorily the different features of HBS behavior observed in these experiments, for both specimens: pore-filling and cementing. Once the main tendencies observed in the experiments have been captured, it may be interesting to explore how the evolution laws and plastic mechanisms proposed in the model work to reproduce the observed behavior. The cementing case is selected for this analysis.

Figure 2a) shows the stress path A-B-C-D on the p-q plane together with the evolution of the yield surface during loading. The model predicts the development of plastic deformations from the beginning of the experiment, with a tendency of the material to harden during the initial stress path A-B-C. Once the point C is reached, the sediment starts to soften with the associated shrinking of the yield surface from the largest size (red one at point C) until smallest and final yield surface (dash line, point D). Figure 2b) presents the deviatoric stress versus axial strain response predicted by the model.

The expansion of the yield surface from A to C is associated with a hardening of the material; while the shrinking of it, from C to D, is related to a softening of the material and stress reduction. The proposed model is able to estimate the portion of the applied stress that is taken by the soil and the one that is supported by the hydrate. In Figure 2b) the total effective stress is presented in red and the portion taken by the hydrate in blue.

Two hardening-softening mechanisms are contemplated in this model. The first one is associated with the preconsolidation pressure, and is considered that p_c depends on the plastic volumetric strain through equation (1). Looking at Figure 2c) it can be seen that when the stress state lies on the 'wet-side' of the yield surface (i.e. when according to the adopted flow rule, the plastic volumetric strains are compressive and positive) additional yielding will induce an increase of p_c (i.e. hardening). However, if the stress state lies on the 'dry-side' of the yield surface (i.e. the volumetric plastic strains are expansive and negative), additional yielding will reduce p_c (i.e. softening).

$$\frac{dp_c}{p_c} = \frac{v}{\lambda - \kappa} d\varepsilon_v^p \tag{1}$$

The other plastic mechanism is related to the sub-loading concept. As explained in Sanchez et al., (2015), and according to Hashiguchi(1989), the sub-loading surface ratio R (with $0 < R \leq 1$) can be incorporated in the definition of the yield surface, leading to:

$$F = \frac{a}{M^2} q^2 - \gamma 3^2 p'^2 + \gamma 3^2 p'^m \left[\mathrm{R}(p_c + p_d)\right]^{2-m} \tag{2}$$

where the evolution of R is controlled by the norm of total plastic deformation ($|d\varepsilon^p|$), leading to an additional increase of the yield surface is hardening take place during yielding. The corresponding evolution law can be written as follows:

$$\mathrm{dR} = -\eta \ln \mathrm{R} \left| d\boldsymbol{\varepsilon}^p \right| \tag{3}$$

The red line in Figure 2.d) corresponds to the evolution of the sub-loading ratio R, and the blue line is related to the evolution of the preconsolidation pressure during the test. The dash line is the effective hardening parameter H of this model (with $H=R(p_c+p_d)$). At beginning of the experiment, p_c increases because the stress state lies on the wet-side of the yield surface (as shown in Figure 1.c, point A). At more advanced stages of the experiment the state states is on the dry-side now and therefore p_c starts to decrease (i.e. there is a softening behavior), while the sub-loading ratio R decreases all the time (i.e. from 0 to 1). In Figure 2.d), the red and blue lines intersect at point C (i.e. peak of deviatoric stress). Until point C, the effective hardening parameter increases (and this implies hardening behavior), which means that the evolution of the sub-loading ratio R dominates the mechanical behavior of the material. However for stress states beyond point C, the effective hardening parameter decreases (i.e. this implies softening

behavior), which means that the softening of p_c dominate the global behavior of sediment after point C.

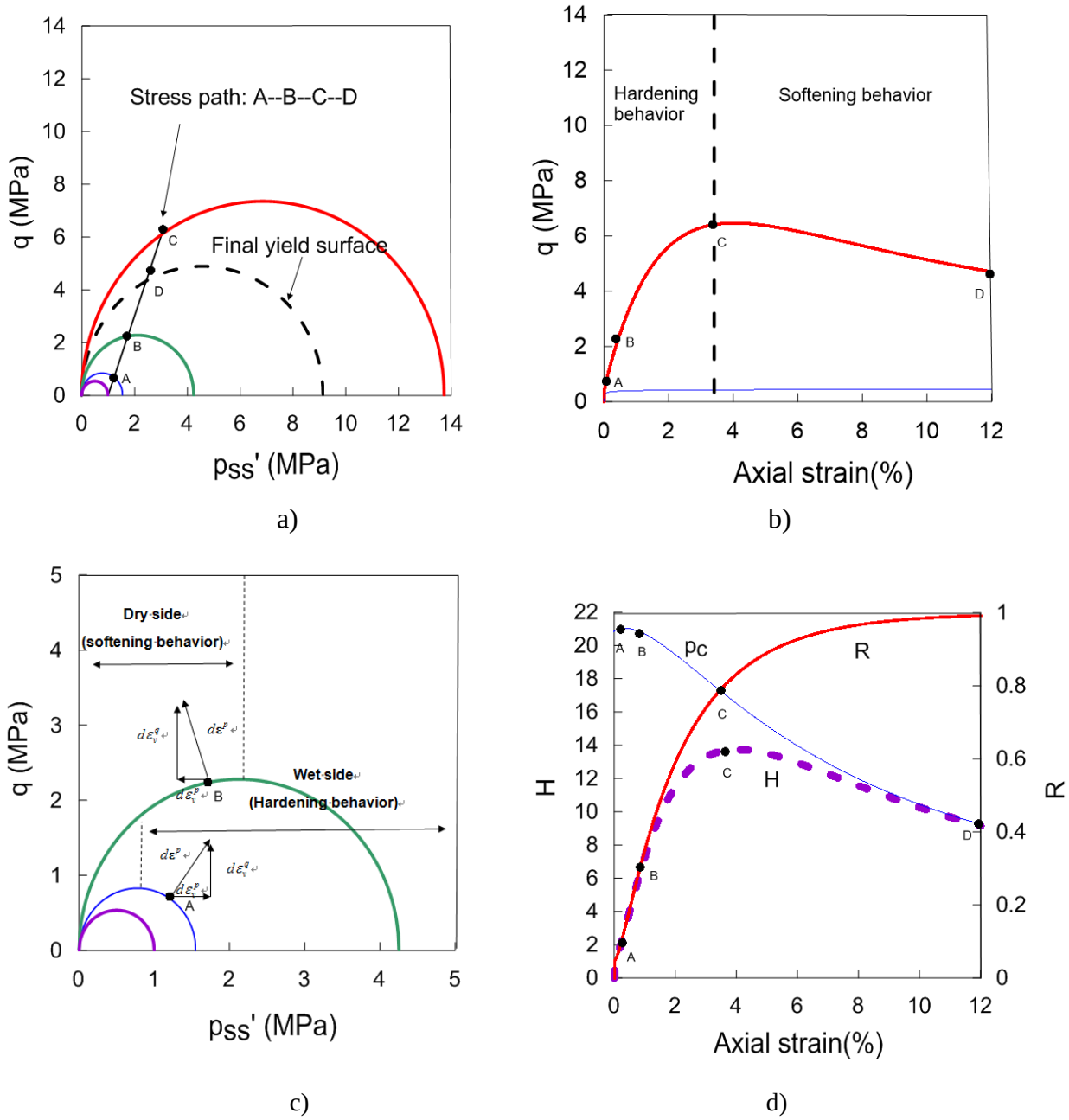

Figure 2 Plastic mechanism considered in HISS-MH model a) stress path and yield surface evolution; b) stress-strain relationship; c) plastic deformations at different stress state; d) evolution of hardening parameters.

1.2 Modeling of HBS behavior during the hydrate dissociation process

The ability of this model to capture the behavior of HBS during hydrate dissociation is evaluated in this section. The model was compared against triaxial tests performed on synthetic samples prepared at similar hydrate saturations and based on the same host sediment (Hyodo et. al., 2013). The samples were firstly sheared to different axial strains (i.e. 1% and 5%) under triaxial compression conditions and then dissociated using the thermal recovery method to learn about the behavior of HBS under these conditions. In order to mimic the formation and dissociation of methane hydrate under deep sea bed, Hyodo et al. (2013) adopted a temperature-controlled high pressure triaxial testing apparatus.

A series of triaxial compression tests on synthetic methane hydrate-bearing sediments were conducted under different conditions. The shear tests were conducted at a strain rate of 0.1% per min under drained conditions. A reduction of the axial load was observed during dissociation process that can be associated with the changes in the sediment structure experienced during this process. Three set of experimental data were selected in this study for the modeling. The related testing conditions are listed in Table 2.

Table 2 Test conditions of methane hydrate dissociation tests

Test conditions						**Test No**	**Remarks**
Production methods	**Consolidation Condition**	**T(°C)**	σ_c' (MPa)	S_h $(\%)$	**Porosity (%)**		
Thermal recovery	Iso	5-20	5	48.7	40.4	1	Dissociation→Shear
			5	47.4	39.9	2	Shear1%→Dissociation→Shear
			5	47.9	39.8	3	Shear5%→Dissociation

Figure 3.a) corresponds to a sample already dissociated and then sheared. The results in Figure 3.b) are related to a soil specimen with hydrates that was sheared until an axial strain of 1% and then dissociated under an axial load of around 8.4 MPa. After dissociation the shearing continued up to an axial strain of 20%. Figure 3c) presents the results of a soil specimen with hydrates sheared up to an axial strain of 5%, and then dissociated under an axial load of around 12 MPa. The three experiments were isotropically consolidated. The dissociation was induced by the thermal recovery method and under an effective confining stress of 5 MPa. The results are presented in terms of deviatoric stress versus axial and volumetric strain versus an axial strain. The reduction of the deviatoric load during hydrate dissociation is quite evident in Figures 3.b) and 3.c).

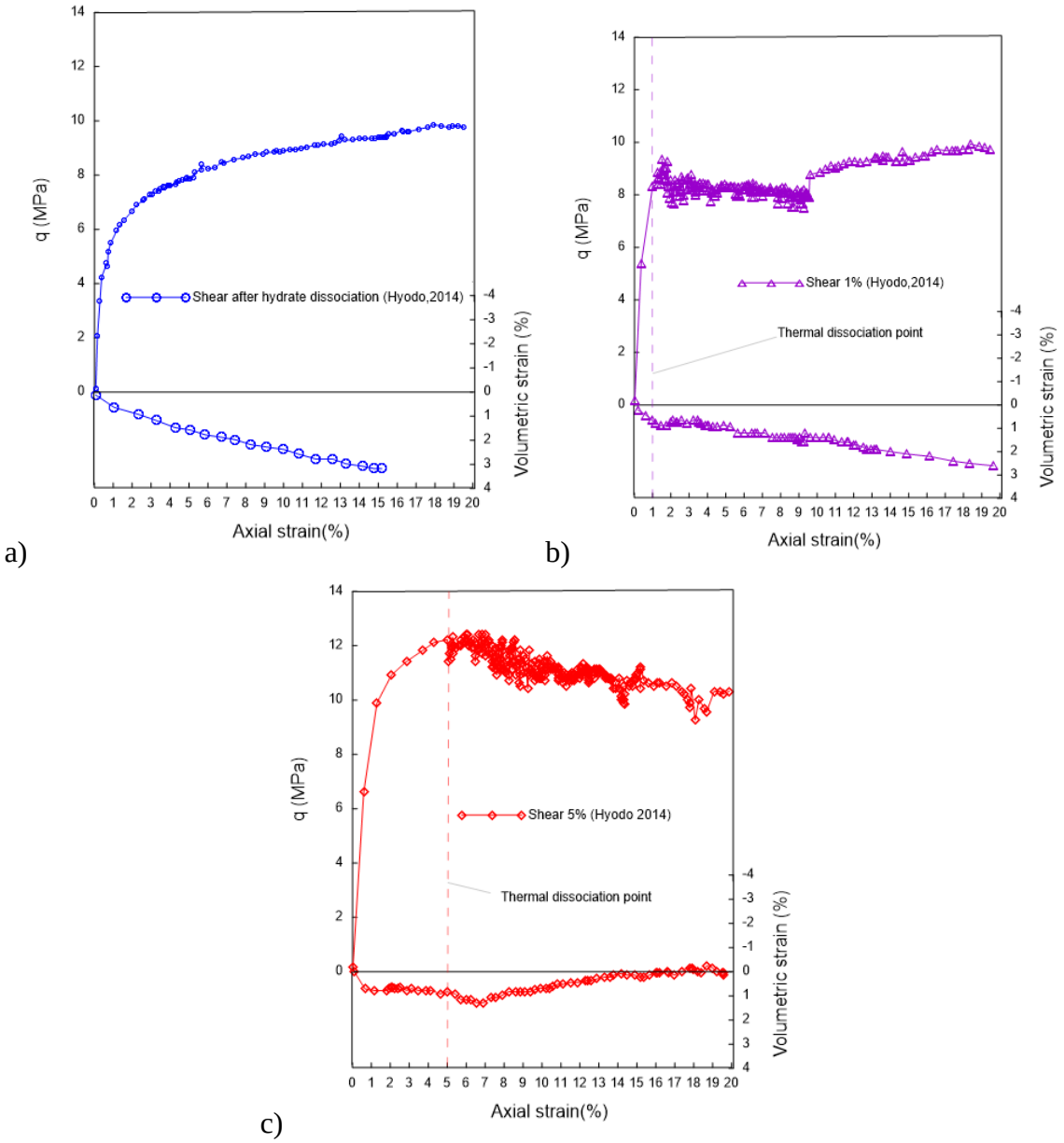

Figure 3 Experimental results of drained triaxial: a) an already dissociated sample, b) specimen sheared until 1% of axial strain, then dissociated and sheared afterwards until 20% axial strain, and c) sample sheared until 5% of axial strain, then dissociated and sheared afterwards aunt l 20% axial strain (Hyodo et. al., 2013).

In order to check the capabilities of the proposed model to reproduce the behavior of samples subjected to dissociation, the tests discussed above were simulated using the HISS-MH model. Figure 4 shows the comparisons between model and experimental results for the already dissociated sample. As expected, the model was able to reproduce very satisfactorily the observations related to both deviatoric stress and volumetric behavior.

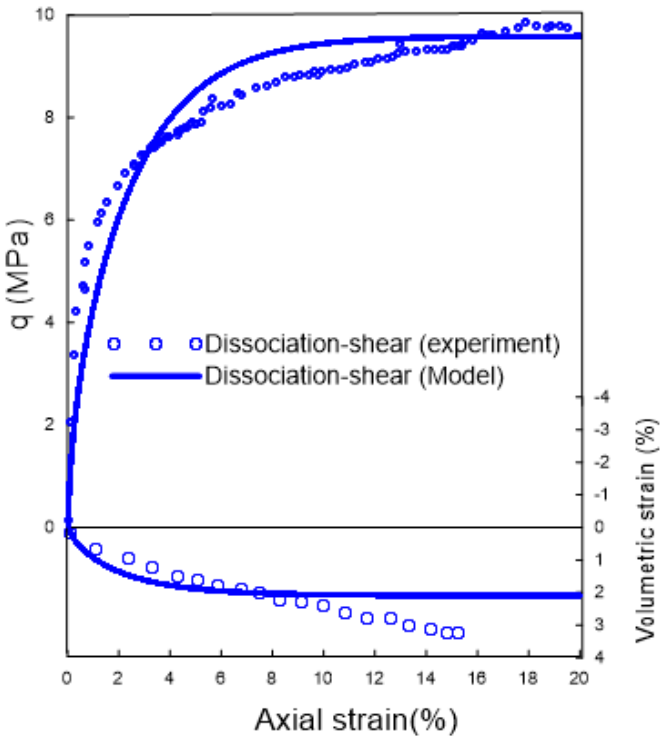

Figure 4. Experimental and numerical results of drained triaxial on an already dissociated sample (experimental data from Hyodo et. al., 2013).

Figure 5 corresponds to the modeling of the sample sheared until an axial deformation of 1%, then dissociated under an axial load of around 8.4 MPa and sheared after the hydrate dissociated completely. The sediment stiffness, deviatoric stress during dissociation and post-dissociation behavior including the residual deviatoric stress were satisfactory modeled, at least the main trends observed in the experiment were properly reproduced. The volumetric strain is slightly under-predicted at large strains.

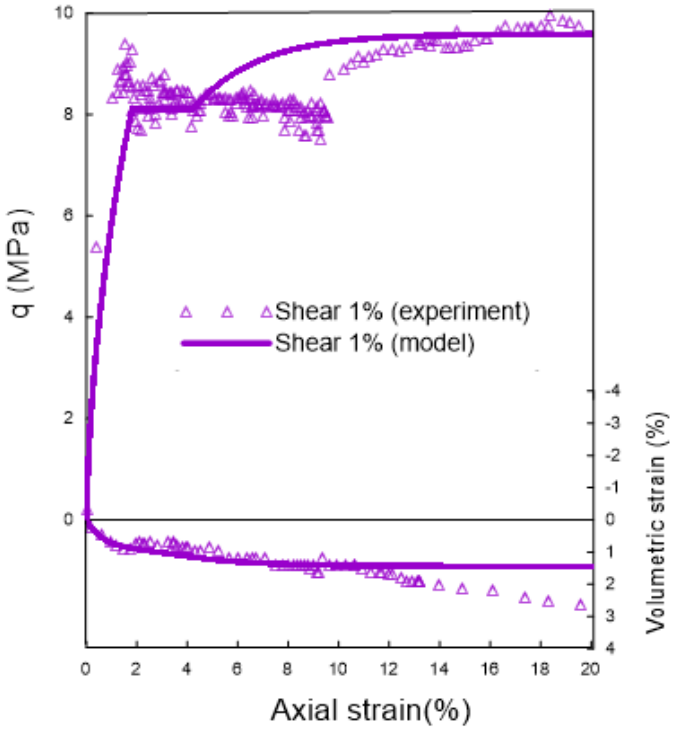

Figure 5. Experimental and numerical results of drained triaxial on a specimen sheared until 1% of axial strain, then dissociated and sheared afterwards until 20% axial strain (experimental data from Hyodo et. al., 2013).

Figure 6 presents the comparisons between experiments and model outputs related to the tests sheared until 5% of axial strain, dissociated then and sheared afterwards again, once the hydrates were totally dissociated. The model was able to match quite well all the experimental observations including: sediment stiffness, maximum deviatoric stress, drop in shear stress and residual deviatoric stress. The results in terms of volumetric strains are also very encouraging; the maximum volumetric strain was well predicted by the model as well as the dilation observed at the latest stages of shearing. All the parameters adopted in this study are listed in Table 3.

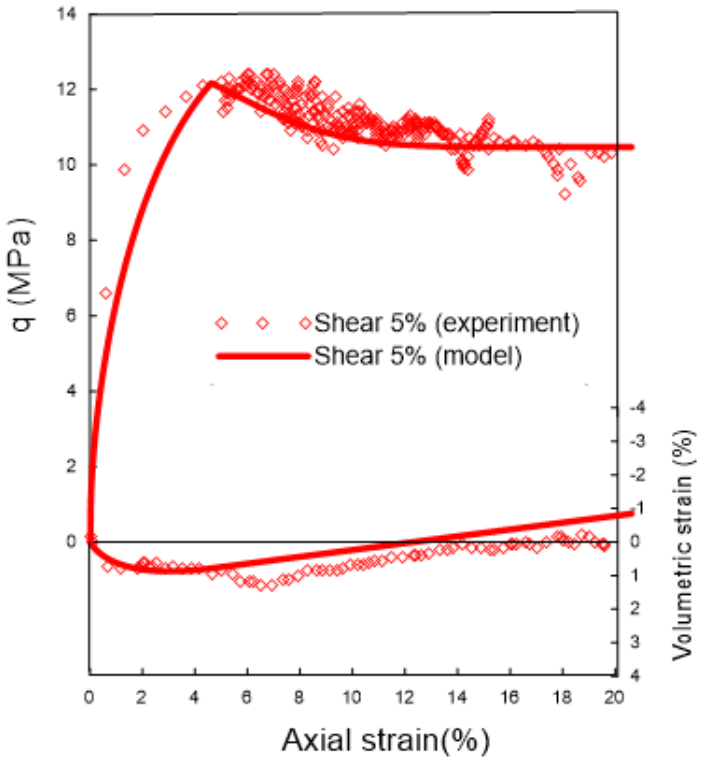

Figure 6. Experimental and numerical results of drained triaxial on a sample sheared until 5% of axial strain, then dissociated and sheared afterwards aunt l 20% axial strain (experimental data from Hyodo et. al., 2013).

Table 3. Parameters adopted in the modeling of HBS specimens

Properties	**Shear after dis**	**Shear 1%**	**Shear 5%**
M	1.17	1.17	1.17
λ	0.012	0.012	0.012
κ	0.004	0.004	0.004
p_c (MPa)	5	5	5
n	3	3	3
a	1	1	1
γ	-1/9	-1/9	-1/9
S_H	0.487	0.474	0.472
α	-	96	96
β	-	1.0	1.0
μ	-	2.9	2.9
η	-	15	15

2 CONCLUSIONS

The HISS-MH model was study in more detail and extended to deal with conditions involving hydrate dissociation. This is a critical aspect for simulating actual gas production scenarios. It was observed that the hardening parameter (R) enable the modeling of the hardening behavior observed at the beginning of the loading step, while the hardening variable (p_c) allow the modeling of the softening behavior observed at advances test stages. The effective hardening parameter H encompasses both plastic mechanisms. After validating the model at constant hydrate saturation conditions, the capability of the model to capture the particular behavior of HBS sample during dissociation was evaluated. The model was compared against tests performed on synthetic samples prepared at similar hydrate saturation and using the same host sediments (Hyodo et. al., 2013). The model was able to capture very satisfactorily the main tendencies observed in the experiments in terms of both stress-strain behavior and volumetric response during shearing and dissociation. .

References

Hyodo, M., J. Yoneda, N. Yoshimoto, and Y. Nakata, *Mechanical and dissociation properties of methane hydrate-bearing sand in deep seabed.* Soils and foundations, 2013. 53(2): p. 299-314.

Masui, A., H. Haneda, Y. Ogata, and K. Aoki. *Effects of methane hydrate formation on shear strength of synthetic methane hydrate sediments*. in *The Fifteenth International Offshore and Polar Engineering Conference*. 2005. International Society of Offshore and Polar Engineers.

Masui, A., H. Haneda, Y. Ogata, and K. Aoki. *Triaxial compression test on submarine sediment containing methane hydrate in deep sea off the coast of Japan* (in Japanese), paper presented at the 41st Annual Conference, Jpn. Geotech. Soc., Kagoshima, 2006, Japan, 12–14 July

Sanchez and Santamaria (2015). "*THCM Coupled Model For Hydrate-Bearing Sediments: Data Analysis and Design of New Field Experiments (Marine and Permafrost Settings*)". DOE Quarterly Research Performance Progress Report (Period ending 07/31/2015).

Uchida, S., K. Soga, and K. Yamamoto, *Critical state soil constitutive model for methane hydrate soil.* Journal of Geophysical Research: Solid Earth (1978–2012), 2012. 117(B3).

PRODUCTS

Publications – Presentations:

- A conference paper was accepted and presented at the 'XV Pan-American Conference on Soil Mechanics and Geotechnical Engineering, hold in Buenos Aires, 15th to 18th November 2015 Title: "Mechanical Modeling of Gas Hydrate Bearing Sediments Using an Elasto-Plastic Framework". Authors: Xuerui Gai, and M. Sanchez.
- An extended abstract entitled 'Numerical and Constitutive Modeling of gas hydrate bearing sediments' was submitted to the "1st International Conference on Geo-Energy and Geo-Environment" to be held in Honk Kong, between 4th and 5th December 2015. Authors: Marcelo Sánchez, Xuerui Gai, J. Carlos Santamarina, Mehdy Teymouri.
- A session on "Hydrate bearing sediments: characterization, modeling and implications on geohazard and gas production", has been accepted for the forthcoming AGU Fall meeting 2015, San Francisco, 14th to 18th December 2015. Marcelo Sanchez is one of the session conveners.
- A journal paper has been prepared. Title: "Mechanical behavior of frozen soils: experimental investigational and constitutive modeling". Authors: Ajay Shastri, Marcelo Sánchez, Moo Y. Lee, and Thomas Dewers.
- A journal paper was submitted to Environmental Geotechnics. Title: "Mechanical Modeling of Gas Hydrate Bearing Sediments Using an Elasto-Plastic Framework". Authors: Xuerui Gai, and M. Sanchez.

Website: Publications (for academic purposes only) and key presentations are included in: http://engineering.tamu.edu/civil/people/msanchez

Technologies or techniques: None at this point.

Inventions, patent applications, and/or licenses: None at this point.

Other products: None at this point.

PARTICIPANTS

Research Team: The current team is shown next.

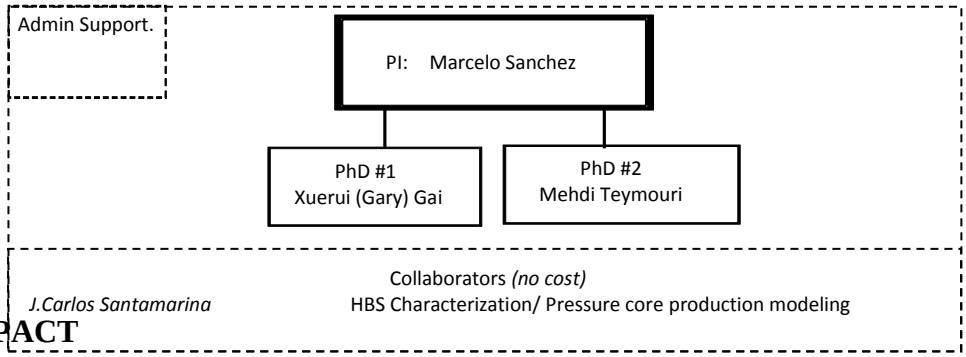

IMPACT

- We can already highlight the computational platform extensively validated in a wide range of coupled thermo-hydro-chemo-mechanical coupled problems (CB_Hydrate).

CHANGES/PROBLEMS:
None so far.

SPECIAL REPORTING REQUIREMENTS:
Nothing to report

BUDGETARY INFORMATION:

Grant No.DE-FE0013889										EXHIBIT 2- COST PLAN/STATUS							
TEES Project 32525-C3870 CE																	
COST PLAN/STATUS																	
				Budget Period 1									Budget Period 2				
	Q1		Q2		Q3		Q4		Q1		Q2		Q3		Q4		
	Enter date range		Enter date range		Enter date range		Enter date range		Enter date range		Enter date range		Enter date range		Enter date range		
Baseline Reporting Quarter	10/1/13- 12/31/13		01/01/14-03/31/14		04/01/14-06/30/14		07/01/14-9/30/14		10/1/14-12/31/2014		01/01/15-03/31/15		04/01/15-06/30/15		07/01/15-9/30/15		
		Cumulative		Cumulative		Cumulative		Cumulative		Cumulative		Cumulative		Cumulative		Cumulative	
	Q1	Total	Q2	Total	Q3	Total	Q4	Total	Q1	Total	Q2	Total	Q3	Total	Q4	Total	
Baseline Cost Plan	$ 40,500.00	$40,500.00	$ 40,500.00	$ 81,000.00	$ 40,500.00	$121,500.00	$ 92,180.00	$ 213,680.00	$ 27,600.00	$241,280.00	$ 27,600.00	$ 268,880.00	$ 27,600.00	$ 296,480.00	$ 92,080.00	$ 388,560.00	
Federal Share	$ 40,500.00	$40,500.00	$ 40,500.00	$ 81,000.00	$ 40,500.00	$121,500.00	$ 92,180.00	$ 213,680.00	$ 27,600.00	$241,280.00	$ 27,600.00	$ 268,880.00	$ 27,600.00	$ 296,480.00	$ 92,080.00	$ 388,560.00	
Non-Federal Share	$ 11,223.00	$11,223.00	$ 11,223.00	$ 22,446.00	$ 11,223.00	$ 33,669.00	$ 11,223.00	$ 44,892.00	$ 11,223.00	$ 56,115.00	$ 11,223.00	$ 67,338.00	$ 11,223.00	$ 78,561.00	$ 11,223.00	$ 89,784.00	
Total Planned	$ 51,723.00	$51,723.00	$ 51,723.00	$ 103,446.00	$ 51,723.00	$155,169.00	$103,403.00	$ 258,572.00	$ 38,823.00	$297,395.00	$ 38,823.00	$ 336,218.00	$ 38,823.00	$ 375,041.00	$103,303.00	$ 388,560.00	
Actual Incurred Costs	$ 5,301.83	$ 5,301.83	$ 13,764.34	$ 19,066.17	$ 33,827.48	$ 52,893.65	$ 51,567.77	$ 104,461.42	$ 80,352.17	$184,813.59	$ 24,626.18	$ 209,439.77	$ 19,260.19	$ 228,699.96	$ 29,858.73	$ 258,558.69	
Federal Share	$ 3,335.02	$ 3,335.02	$ 9,848.68	$ 13,183.70	$ 10,170.37	$ 23,354.07	$ 58,205.62	$ 81,559.69	$ 92,208.79	$173,768.48	$ 31,359.66	$ 205,128.14	$ 19,260.19	$ 224,388.33	$ 29,812.17	$ 254,200.50	
Non-Federal Share	$ 5,182.96	$ 5,182.96	$ 20,751.77	$ 25,934.73	$ 20,743.19	$ 46,677.92	$ 29,262.19	$ 75,940.11	$ -	$ 75,940.11	$ -	$ 75,940.11	$ 8,833.66	$ 84,773.77	$ -	$ 84,773.77	
Total Incurred costs	$ 8,517.98	$ 8,517.98	$ 30,600.45	$ 39,118.43	$ 30,913.56	$ 70,031.99	$ 87,467.81	$ 157,499.80	$ 92,208.79	$249,708.59	$ 31,359.66	$ 281,068.25	$ 28,093.85	$ 309,162.10	$ 29,812.17	$ 338,974.27	
Varience	$ 43,205.02	$43,205.02	$ 21,122.55	$ 64,327.57	$ 20,809.44	$ 85,137.01	$ 15,935.19	$ 101,072.20	$(53,385.79)	$ 47,686.41	$ 38,823.00	$ 55,149.75	$ 10,729.15	$ 65,878.90	$ 73,490.83	$ 49,585.73	
Federal Share	$ (1,966.81)	$ (1,966.81)	$ (3,915.66)	$ (5,882.47)	$ (23,657.11)	$ (29,539.58)	$ 6,637.85	$ (22,901.73)	$ 11,856.62	$ (11,045.11)	$ 6,733.48	$ (4,311.63)	$ -	$ (4,311.63)	$ 4,358.19	$ 46.56	
Non-Federal Share	$ 6,040.04	$ 6,040.04	$ (9,528.77)	$ (3,488.73)	$ (9,520.19)	$ (13,008.92)	$ (40,485.19)	$ (53,494.11)	$ 11,223.00	$ (42,271.11)	$ 6,733.48	$ (35,537.63)	$ 2,389.34	$ (33,148.29)	$ 11,223.00	$ (21,925.29)	
Total Varience	$ 4,073.23	$ 4,073.23	$ (13,444.43)	$ (9,371.20)	$ (33,177.30)	$ (42,548.50)	$ (33,847.34)	$ (76,395.84)	$ 23,079.62	$ (53,316.22)	$ 13,466.96	$ (39,849.26)	$ 2,389.34	$ (37,459.92)	$ 15,581.19	$ (21,878.73)	

National Energy Technology Laboratory

626 Cochrans Mill Road
P.O. Box 10940
Pittsburgh, PA 15236-0940

3610 Collins Ferry Road
P.O. Box 880
Morgantown, WV 26507-0880

13131 Dairy Ashford Road, Suite 225
Sugar Land, TX 77478

1450 Queen Avenue SW
Albany, OR 97321-2198

Arctic Energy Office
420 L Street, Suite 305
Anchorage, AK 99501

Visit the NETL website at:
www.netl.doe.gov

Customer Service Line:
1-800-553-7681